# NEAT1 long noncoding RNA regulates transcription via protein sequestration within subnuclear bodies

Tetsuro Hirose[a,b], Giorgio Virnicchi[c], Akie Tanigawa[b], Takao Naganuma[b], Ruohan Li[d], Hiroshi Kimura[e], Takahide Yokoi[f], Shinichi Nakagawa[g], Marianne Bénard[h], Archa H. Fox[d], and Gérard Pierron[c]

[a]Institute for Genetic Medicine, Hokkaido University, Sapporo 060-0815, Japan; [b]Biomedical Research Institute, National Institute of Advanced Industrial Science and Technology, Tokyo 135-0064, Japan; [c]Centre National de la Recherche Scientifique, UMR-8122, Institut Gustave Roussy, Villejuif 94805, France; [d]Western Australian Institute for Medical Research, Center for Medical Research, University of Western Australia, Perth, Western Australia 6000, Australia; [e]Graduate School of Frontier Biosciences, Osaka University, Suita 565-0871, Japan; [f]Hitachi, Kokubunji, Tokyo 185-8601, Japan; [g]RIKEN Advanced Institute, Wako 351-0198, Japan; [h]Centre National de la Recherche Scientifique, FRE 3402, UPMC Université Paris 06, Paris 75 252, France

**ABSTRACT Paraspeckles are subnuclear structures formed around nuclear paraspeckle assembly transcript 1 (NEAT1)/MENε/β long noncoding RNA (lncRNA). Here we show that paraspeckles become dramatically enlarged after proteasome inhibition. This enlargement is mainly caused by NEAT1 transcriptional up-regulation rather than accumulation of undegraded paraspeckle proteins. Of interest, however, using immuno–electron microscopy, we find that key paraspeckle proteins become effectively depleted from the nucleoplasm by 50% when paraspeckle assembly is enhanced, suggesting a sequestration mechanism. We also perform microarrays from NEAT1-knockdown cells and find that NEAT1 represses transcription of several genes, including the RNA-specific adenosine deaminase B2 (ADARB2) gene. In contrast, the NEAT1-binding paraspeckle protein splicing factor proline/glutamine-rich (SFPQ) is required for ADARB2 transcription. This leads us to hypothesize that ADARB2 expression is controlled by NEAT1-dependent sequestration of SFPQ. Accordingly, we find that ADARB2 expression is strongly reduced upon enhanced SFPQ sequestration by proteasome inhibition, with concomitant reduction in SFPQ binding to the ADARB2 promoter. Finally, NEAT1$^{-/-}$ fibroblasts are more sensitive to proteasome inhibition, which triggers cell death, suggesting that paraspeckles/NEAT1 attenuates the cell death pathway. These data further confirm that paraspeckles are stress-responsive nuclear bodies and provide a model in which induced NEAT1 controls target gene transcription by protein sequestration into paraspeckles.**

**Monitoring Editor**
A. Gregory Matera
University of North Carolina

Received: Oct 1, 2013
Accepted: Oct 24, 2013

This article was published online ahead of print in MBoC in Press (http://www.molbiolcell.org/cgi/doi/10.1091/mbc.E13-09-0558) on October 30, 2013.

Address correspondence to: Tetsuro Hirose (hirose@igm.hokudai.ac.jp), Archa H. Fox (archa.fox@waimr.uwa.edu.au), Gérard Pierron (gerard.pierron@igr.fr).

Abbreviations used: ADARB2, adenosine deaminase RNA-specific B2; ASO, antisense oligonucleotide; EU, 5-ethynyl uridine; lncRNA, long noncoding RNA; MEF, mouse embryonic fibroblast; NEAT1, nuclear paraspeckle assembly transcript 1; qRT-PCR, quantitative reverse transcription-PCR; RNAPII, RNA polymerase II; SFPQ, splicing factor proline/glutamine-rich.

© 2014 Hirose *et al.* This article is distributed by The American Society for Cell Biology under license from the author(s). Two months after publication it is available to the public under an Attribution–Noncommercial–Share Alike 3.0 Unported Creative Commons License (http://creativecommons.org/licenses/by-nc-sa/3.0).

"ASCB®," "The American Society for Cell Biology®," and "Molecular Biology of the Cell®" are registered trademarks of The American Society of Cell Biology.

## INTRODUCTION

The nucleus of mammalian cells is highly organized. It is composed of distinct nuclear bodies—membrane-less organelles containing specific proteins or RNAs characteristic of particular nuclear processes (Spector, 2006). Paraspeckles are nuclear bodies detected in mammalian cells as a variable number of foci found in close proximity to nuclear speckles (Visa *et al.*, 1993; Fox *et al.*, 2002). Paraspeckles were initially defined as foci enriched in characteristic RNA-binding proteins, including the three mammalian *Drosophila melanogaster* behavior and human splicing (DBHS) proteins, PSPC1, NONO (p54nrb), and splicing factor proline/glutamine-rich (SFPQ; PSF; Fox *et al.*, 2002, 2005; Prasanth *et al.*, 2005). Beyond their localization in

paraspeckles, the DBHS proteins have been implicated in numerous nuclear processes, including transcriptional control, RNA processing, and DNA repair (Shav-Tal and Zipori, 2002; Dong *et al.*, 2007; Kaneko *et al.*, 2007; Bond and Fox 2009; Li *et al.*, 2009; Heyd and Lynch, 2010).

A number of relatively abundant long noncoding RNAs (lncRNAs) have been found to localize to specific nuclear bodies (Clemson *et al.*, 1996, 2009; Hutchinson *et al.*, 2007; Sone *et al.*, 2007; Sasaki *et al.*, 2009; Sunwoo *et al.*, 2009; Tripathi *et al.*, 2010; Zheng *et al.*, 2010; Yang *et al.*, 2011). Prominent among these is the nuclear paraspeckle assembly transcript 1 (NEAT1) lncRNA, which is found to localize specifically to paraspeckles, where it forms an essential structural component (Chen and Carmichael, 2009; Clemson *et al.*, 2009; Sasaki *et al.*, 2009; Sunwoo *et al.*, 2009). The human NEAT1 gene generates two RNA transcripts, 3700-nucleotide (nt) NEAT1_1 and 23,000-nt NEAT1_2 (also known as MENε and MENβ, respectively). NEAT1_2, but not NEAT1_1, was demonstrated to be a potent RNA component for de novo paraspeckle construction (Naganuma *et al.*, 2012). The organization of NEAT1 within paraspeckles has been precisely delineated by electron microscopy, revealing that the 5′ region (common to both isoforms), as well as the 3′ end of NEAT1_2, is located at the paraspeckle periphery, whereas only the NEAT1_2 middle region is located in the paraspeckle interior (Souquere *et al.*, 2010).

We recently identified 35 new paraspeckle proteins (PSPs), most of which contain canonical RNA-binding motifs. RNA interference (RNAi) analysis revealed that seven PSPs are essential for paraspeckle formation (Naganuma *et al.*, 2012). These nucleoplasmic PSPs rapidly associate with and stabilize NEAT1 as it is transcribed, forming a network of interactions resulting in mature paraspeckles (Sasaki *et al.*, 2009; Mao *et al.*, 2011; Naganuma *et al.*, 2012).

Although considerable progress has been made into paraspeckle composition, formation, and molecular organization, the biological function of paraspeckles and the roles of NEAT1 lncRNAs remain to be fully elucidated. It was shown that CTN-RNA, an isoform of mCAT2 mRNA, is localized in paraspeckles (Prasanth *et al.*, 2005). The CTN-RNA 3′ untranslated region (UTR) contains an inverted repeat capable of forming intramolecular double-stranded RNAs that are adenosine-to-inosine (A-to-I) edited. Intriguingly, the CTN-RNA 3′UTR is cleaved upon certain stresses, leading to the export of processed mCAT2 mRNA for translation. Thus paraspeckles are believed to suppress the expression of hyperedited transcripts through nuclear retention (Prasanth *et al.*, 2005). Consistent with this, NEAT1 knockdown and dissolution of paraspeckles resulted in relocation of nuclear-retained mRNAs to the cytoplasm (Chen and Carmichael, 2009). These data suggest that paraspeckles control nucleocytoplasmic transport of mRNAs that are A-to-I edited by adenosine deaminases acting on RNA (ADARs). However, considering the variety of different proteins accumulated in paraspeckles, it is likely the paraspeckles have additional functions other than nuclear retention of mRNAs.

NEAT1 induction and paraspeckle enlargement have been reported in various conditions, including viral infection and myotube differentiation (Saha *et al.*, 2006; Sunwoo *et al.*, 2009; Zhang *et al.*, 2013). Here we provide evidence that NEAT1 is highly up-regulated by proteasome inhibition, leading to paraspeckle elongation and measurable sequestration of NEAT1-bound transcription factors within the enlarged paraspeckles. As a consequence, we show that expression of several paraspeckle-target genes is altered. We also provide evidence that in the absence of paraspeckles, as in NEAT1-knockout mouse embryonic fibroblasts (MEFs), cells are more sensitive to proteasome inhibitor–mediated cell death, suggesting a pro-survival role for paraspeckles in stress conditions.

## RESULTS

### Proteasome inhibition induces grossly enlarged paraspeckles

To uncover the role of paraspeckles, we searched for conditions in which paraspeckle function might be enhanced. We found that paraspeckles were markedly enlarged when cells were treated with proteasome inhibitors. By a combination of RNA–fluorescence in situ hybridization (FISH) and immunostaining to simultaneously detect NEAT1 and one of the paraspeckle marker proteins, PSPC1, we observed enlarged paraspeckles in HeLa cells treated with 5 μM MG132 for 6 or 14 h (Figure 1A and Supplemental Figure S1). In all of the enlarged paraspeckles observed, the NEAT1 and PSPC1 signals completely overlapped.

Electron microscopic (EM) studies revealed that these enlarged paraspeckles correspond to clusters of typical paraspeckles (Figure 1B). Even after 17 h of MG132 treatment, as in Figure 1B, paraspeckle ultrastructure was unchanged as compared with control HeLa cells, but their frequency was markedly increased. When HeLa cells were treated with the structurally different proteasome inhibitor bortezomib (100 nM, 17 h), a similar increase of paraspeckle frequency was observed (Figure 1B), indicating a true dependence on proteasome inhibition in this phenomenon. Paraspeckle clustering, as seen in the EM studies, suggested elongated and twisted structures cut several times by thin sectioning. Thus we measured the long and short axes (*Lx* and *Sx*) of 120 paraspeckles in EM sections from control and MG132-treated HeLa cells (examples shown in Figure 1C). Plotting the values by increasing *Lx* (Figure 1D) illustrates a significant MG132-dependent paraspeckle elongation (mean length of 638 nm for MG132- treated paraspeckles vs. 464 nm for control, $p < 0.001$), whereas the constant *Sx* values indicate a similarly constrained diameter in control and treated cells (mean 320 ± 36 and 312 ± 41 nm, respectively). Thus the enlargement of paraspeckles that we observed was due to significant elongation.

By immunogold EM (I-EM), we analyzed the distribution of proteins that accumulate upon proteasome inhibition and found no indication of enrichment in paraspeckles. After MG132 or bortezomib treatment, dense cytoplasmic and nuclear aggregates (absent from control cells) were conspicuous. Cytoplasmic aggregates formed around centrioles and were heavily labeled with an anti-ubiquitin antibody, indicative of aggresomes (Supplemental Figure S2). Nuclear aggregates, highly enriched in ubiquitin conjugates and SUMOylated proteins, were always found closely associated with the nucleolus (Figure 2A) but, strikingly, did not overlap with paraspeckles (Figure 2A). Finally, the nuclear protein aggregates condensed into large, dense bodies concentrating ubiquitin and SUMO-1 and SUMO-2/3 at their periphery (Figure 2B). These MG132-induced nuclear bodies were surrounded by a thin layer of promyelocytic leukemia (PML) protein. Thus formation of elongated paraspeckles and the accumulation of proteins by proteasome inhibition are compartmentalized, unrelated events.

### Transcriptional up-regulation of NEAT1 causes elongated paraspeckle formation in proteasome-inhibited cells

In a search for factors controlling elongated paraspeckle formation, we determined by Western blotting that seven PSPs, each essential for paraspeckle formation, did not increase with MG132 treatment (Figure 2C). By I-EM, we determined that endogenous NONO, CPSF6, and SFPQ were similarly distributed and similarly abundant within the paraspeckles of control (dimethyl sulfoxide [DMSO]) and MG132-treated HeLa cells (illustrated in Figure 2D and quantified in Figure 2E). Taken together, these data indicate that elongated paraspeckles are unlikely to result from an unusual

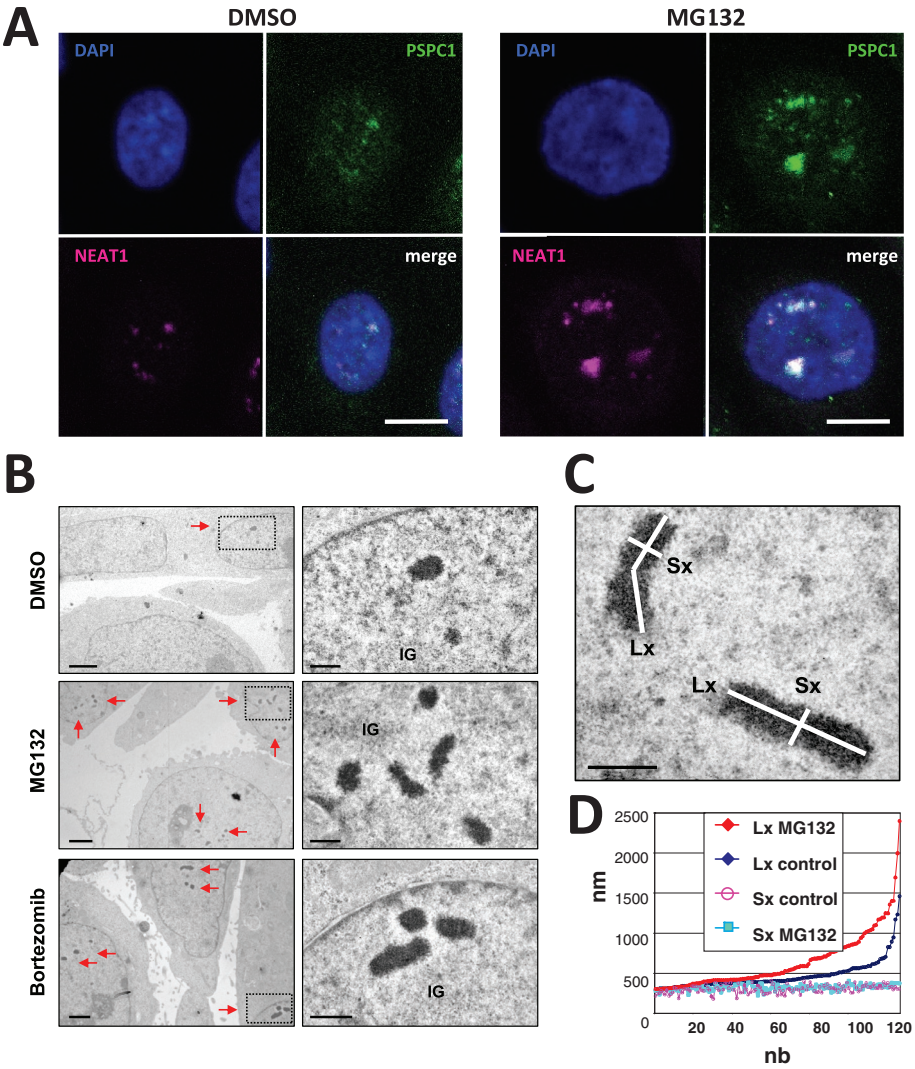


FIGURE 1: Proteasome inhibition results in paraspeckle elongation. (A) Paraspeckle enlargement upon proteasome inhibition. HeLa cells were treated with DMSO or 5 μM MG132 for 17 h. The paraspeckles were detected by RNA-FISH of NEAT1 lncRNAs (magenta) combined with immunofluorescence of PSPC1 (green). Scale bar, 10 μm. (B) Paraspeckle ultrastructure upon proteasome inhibition. HeLa cells treated with DMSO, 5 μM MG132, or 100 nM bortezomib for 17 h were analyzed by transmission EM after Epon embedding. Left, large fields; bar, 2 μm. Right, enlargement of dashed rectangles; bar, 0.5 μm. Red arrows, paraspeckle clusters; IG, interchromatin granule. (C) Size measurements of paraspeckle in control and MG132-treated HeLa cells (5 μM, 17 h). Short and long axes (*Sx* and *Lx*) were defined for 120 paraspeckles in each sample from Epon-embedded HeLa cells. Bar, 0.5 μm. (D) Dimensions were plotted by increasing *Lx* values, showing similar *Sx* values in both samples, whereas *Lx* values were augmented in the MG132-treated cells.

accumulation or repositioning of PSPs. Next we investigated whether levels of the essential paraspeckle RNA, NEAT1, were affected by proteasome inhibition. RNase protection assays and quantitative reverse transcription-PCR (qRT-PCR) measurements of NEAT1_1 and NEAT1_2 levels revealed that both isoforms significantly increased upon MG132 treatment (Figure 3, A and B, showing greater than eightfold increase in NEAT1 after 17 h MG132). RNase protection assays showed that the kinetics of up-regulation is faster in NEAT1_2 than NEAT1_1 (Figure 3, A and B). To investigate whether this increase was transcriptional or posttranscriptional, we quantified the newly synthesized nascent NEAT1 ncRNA. For capturing nascent RNAs, HeLa cells were pulse labeled with 5-ethynyl uridine (EU) for 1 h, and the EU-incorporated RNAs were biotinylated and purified with streptavidin-conjugated beads. qRT-PCR of the captured RNAs revealed that nascent NEAT1 RNA levels were similar to total RNA (steady-state levels) in control and MG132-treated cells (Figure 3C), indicating that the increased NEAT1 was resulting from new transcripts. Chromatin immunoprecipitation (ChIP) with anti–RNA polymerase II (RNAPII) phosphorylated at serine 5 in the carboxy-terminal domain (phospho-CTD-ser5) showed MG132 treatment resulted in a significant increase of RNAPII phospho-CTD-ser5 bound within the NEAT1 promoter but not the glyceraldehyde-3-phosphate dehydrogenase (GAPDH) promoter (Figure 3D). Further, a luciferase reporter gene driven by the human NEAT1 promoter was significantly activated by MG132 treatment, whereas a control SV40 promoter was not (Figure 3E).

Finally, by in situ hybridization in the EM, we determined that the known distinct location of each NEAT1 isoform within paraspeckles (Souquere *et al.*, 2010) was maintained upon MG132 stimulation. As shown in Supplemental Figure S3, NEAT1_1 and the indistinguishable 5′ end of NEAT1_2 were, with the 3′ end of NEAT1_2, restricted to the periphery of the paraspeckle. In contrast, the internal sequence of NEAT1_2 (labeled as D1 in Supplemental Figure S3) was located within paraspeckles in control and MG132-treated HeLa cells. Collectively these data show that paraspeckle elongation upon proteasome inhibition is driven by transcriptional up-regulation of the NEAT1 gene rather than paraspeckle protein accumulation or a change in ultrastructural organization of key paraspeckle components.

### SFPQ and NONO are sequestrated within elongated paraspeckles upon proteasome inhibition

We next examined the relative amounts of paraspeckle proteins trapped within these MG132-induced elongated paraspeckles. Labeling densities of NONO, SFPQ, and CPSF6, as measured by I-EM in Figure 2, were comparable in paraspeckles of control and MG132-treated HeLa cells. However, considering the fourfold to fivefold increased frequency of paraspeckles on thin sections of proteasome-inhibited cells (see *Materials and Methods*), our results imply that four to five times more of NONO, CPSF6, and SFPQ are contained within the MG132-induced elongated paraspeckles. We next asked whether this increased inclusion within the enlarged paraspeckles is sufficient to deplete a significant proportion of these proteins from the nucleoplasm. By I-EM, we compared labeling densities of NONO or SFPQ in cytoplasmic, nucleoplasmic, and paraspeckle areas in control and MG132-treated cells. Our results indicate that in MG132-treated cells the nucleoplasmic pools of SFPQ and NONO were depleted by roughly 50%

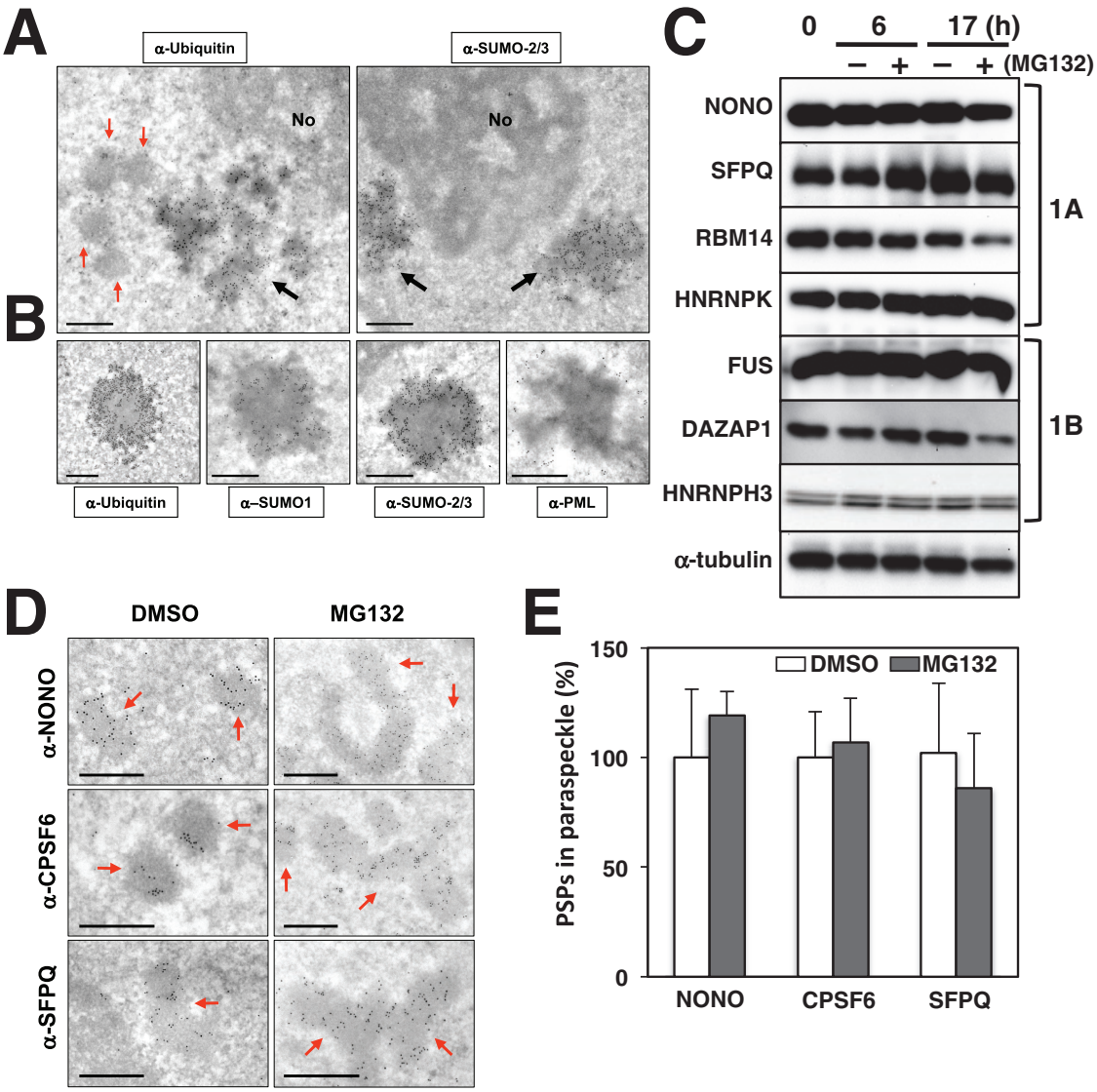


FIGURE 2: Proteasome inhibition does not result in accumulation of ubiquitinated proteins or reorganization of protein components within paraspeckles. (A) I-EM detection of ubiquitinated and SUMOylated proteins accumulating upon proteasome inhibition (thin sections of Lowicryl-embedded HeLa cells, MG132-treated 5 μM, 17 h). Left, dense aggregates (black arrow) of nuclear ubiquitinated proteins are formed in the vicinity of the nucleolus (No). In contrast, the expanded paraspeckles (red arrows) do not contain significant amount of ubiquitin. Right, SUMOylated proteins also accumulate in the ubiquitin-positive nuclear aggregates. Bars, 0.5 μm. (B) In some nuclear sections, MG132-induced protein aggregates form well-defined nuclear bodies, highly enriched at their periphery in ubiquitin- and SUMO-conjugated proteins and surrounded by a thin layer of PML protein. Bars, 0.5 μm. (C) The PSP levels were largely constant upon MG132 treatment. Seven essential PSPs (defined as those proteins whose knockdown in HeLa cells result in loss of paraspeckles) were detected in cells treated with DMSO or MG132 for 6 or 17 h by Western blotting. Category 1A proteins (1A) are required for both paraspeckle integrity and NEAT1_2 accumulation, whereas category 1B proteins (1B) do not affect NEAT1_2 levels but are required for paraspeckles. α-Tubulin is the control. (D) Abundance and distribution of NONO, CPSF6, and SFPQ in control and MG132-amplified paraspeckles was determined by I-EM. Red arrows indicate highly labeled paraspeckles. Bars, 0.5 μm. (E) Labeling densities (gold particles/μm$^2$) of the three PSPs were quantified from the images shown in D, displaying a constant level of protein per unit surface of paraspeckle. At least 20 paraspeckles or 500 gold particles were counted for each sample. Bars, 0.5 μm.

compared with control values (Figure 4). In contrast, relatively constant labeling values were obtained within the cytoplasmic and paraspeckle compartments. We conclude that NEAT1 up-regulation by proteasome inhibition leads to NONO and SFPQ sequestration within enlarged paraspeckles. Given that the nucleoplasmic pools of SFPQ and NONO were affected by 50%, in a manner akin to haploinsufficiency, we anticipated that NONO and SFPQ sequestration within paraspeckles was likely to have pronounced effects on transcription.

### Identification of the adenosine deaminase RNA–specific B2 gene as a paraspeckle-target gene

To complement these investigations into paraspeckle enlargement, we then examined paraspeckle loss. Specific depletion of NEAT1

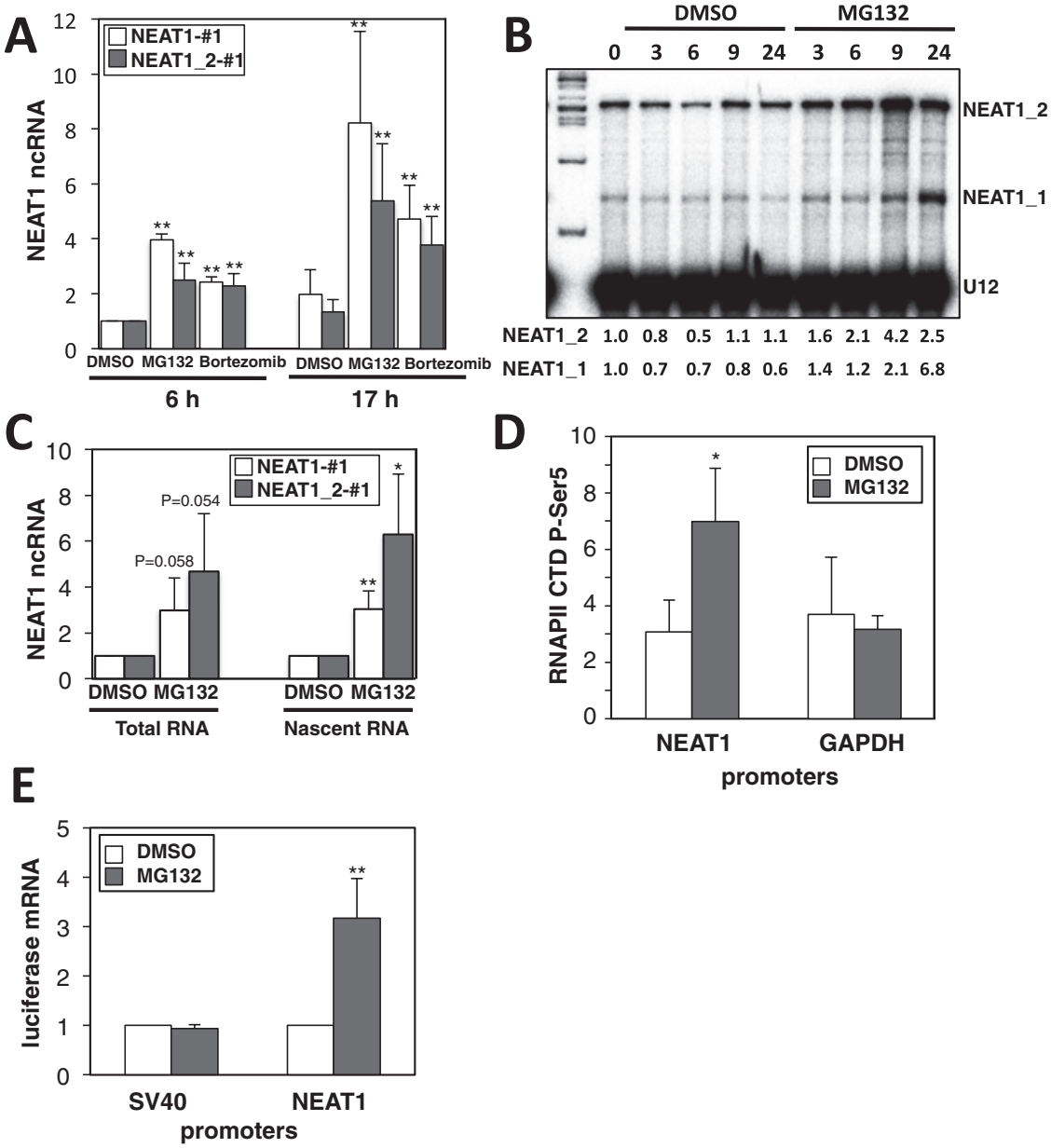


FIGURE 3: Proteasome inhibition activates NEAT1 lncRNA synthesis. (A, B) Proteasome inhibition results in elevation of NEAT1 lncRNA levels detected by qRT-PCR (A) and RNase protection assay (RPA; B). Quantitation of the RNase-protected bands is shown at the bottom. (C) Proteasome inhibition elevates the level of the newly synthesized nascent NEAT1 lncRNAs. Total and EU-labeled nascent RNAs prepared from the cells treated with DMSO or MG132 for 6 h were used for quantitation of NEAT1. For qRT-PCR, two primer sets corresponding to the NEAT1_1/1_2-overlapping region (NEAT1-#1) and the NEAT1_2-specific region (NEAT1_2-#1) were used. (D) Elevated binding of RNAPII phospho CTD serine 5 at the NEAT1 promoter in MG132-treated cells. Chromatin immunoprecipitation with αRNAPII phospho CTD serine 5 antibody was carried out in cells treated with DMSO or MG132 for 6 h. Levels of coimmunoprecipitated DNA fragments were quantified by qPCR with primer sets that span promoter regions of NEAT1 and glyceraldehyde-3-phosphate dehydrogenase (GAPDH) as control. $^{**}p < 0.01$, $^{*}p < 0.05$. (E) The NEAT1 promoter is activated by MG132. The graph shows qPCR of luciferase cDNA, relative to GAPDH, normalized to the control (untreated sample). RNA was extracted from MG132- and DMSO-treated HeLa cells transiently transfected 48 h before with plasmids encoding luciferase driven by the promoters as indicated. Error bars are SD as a result of two biological replicates.

with a chimeric antisense oligonucleotide (ASO) leads to disintegration of paraspeckles (Sasaki *et al.*, 2009). To identify paraspeckle-target genes, we carried out microarray analyses using total RNA samples from HeLa cells treated with control (GFP) or NEAT1 ASO (#12) for 6, 12, and 24 h (Figure 5A). A modest total of 51 genes overrepresented or underrepresented greater than twofold upon NEAT1 reduction were detected from these three time points (Supplemental Table S1). We confirmed this result with qRT-PCR for several genes up-regulated by NEAT1 depletion (Figure 5B) and found that they were reproducibly up-regulated in cells treated with different NEAT1 ASOs (#12 and #17; Supplemental Figure S4 shows the efficacy of the ASOs on NEAT1 levels). Given the intriguing link between one of these genes—the adenosine deaminase RNA-specific B2 (ADARB2) gene function in RNA editing—and the previous observation that

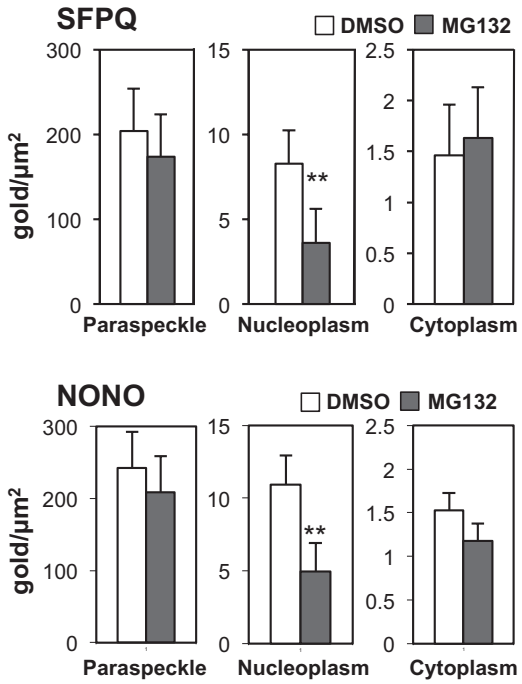


FIGURE 4: MG132 affects SFPQ and NONO nuclear distribution, resulting in depleted nucleoplasmic levels of the proteins. SFPQ or NONO density was determined by I-EM as gold particles/µm$^2$ within paraspeckles, the surrounding nucleoplasm, and the cytoplasm of DMSO- and MG132-treated (5 µM, 17 h) HeLa cells. Although the proteins occur at different density values in the three locations (note the different values on the *y* axes), only the nucleoplasmic pool of SFPQ and NONO was specifically depleted with MG132, in parallel with paraspeckle enlargement under this condition. Densities were calculated on 120 and 140 µm$^2$ of cytoplasm, 93 and 92 µm$^2$ of nucleoplasm, and 33 and 51 paraspeckles in DMSO and MG132 cells, respectively, for SFPQ. Corresponding values for NONO are 76 and 75, 108 and 92, and 25 and 45.

paraspeckles were involved in retaining edited RNA, we chose ADARB2 for detailed characterization of a paraspeckle-target gene. First, Northern blot hybridization detected four ADARB2 mRNA isoforms (3–8.5 kb) generated by different polyadenylation sites in HeLa cells, all of which increased upon NEAT1 lncRNA elimination (ΔNEAT1) with two different ASOs (lanes #12 and #17 in Figure 5C), suggesting elevation of ADARB2 transcription rather than altered posttranscriptional regulation at heterogeneous 3′ ends. To investigate this possibility, we quantified the level of nascent ADARB2 mRNA in control and ΔNEAT1 cells. The pulse-labeling experiment (as in Figure 3C) revealed that nascent ADARB2 mRNA was elevated similar to that of total ADARB2 mRNAs (Figure 5D). The stability of ADARB2 mRNA (measured by degradation after actinomycin D treatment) was unaltered in the presence and absence of NEAT1 (CDS in Figure 5E). We also determined that the subcellular localization of ADARB2 mRNA was not altered when NEAT1 was knocked down (Supplemental Figure S5). These results argue that ADARB2 is a paraspeckle-target gene, transcriptionally up-regulated when NEAT1 levels and paraspeckle integrity are lowered.

### The paraspeckle protein SFPQ is required for transcription of ADARB2

In a search for a link between NEAT1 levels, paraspeckle assembly, and ADARB2 gene transcription, we independently silenced each of the 32 PSPs that are expressed in HeLa cells, using validated small interfering RNA (siRNA) in which >70% knockdown is achieved (Naganuma *et al.*, 2012). qRT-PCR of ADARB2 mRNA levels revealed that SFPQ and, to a lesser extent, HNRNPH1 were required for ADARB2 gene expression (siSFPQ: ADARB2 <5% of control; siHNRNPH1: ~20%; Figure 6A). This effect was not observed in control GAPDH mRNA (Supplemental Figure S6). To identify the stage of ADARB2 gene expression that is facilitated by SFPQ and HNRNPH1, we captured newly synthesized mRNAs as in Figure 5D in control, siSFPQ, and siHNRNPH1 cells. Nascent ADARB2 mRNA levels were markedly reduced in both siSFPQ and siHNRNPH1 cells (Figure 6B). Finally, Northern blotting showed that all isoforms of ADARB2 mRNA were strongly reduced upon SFPQ elimination (Figure 6C). Taken together, these results suggest that SFPQ and HNRNH1 have an activating role in ADARB2 gene transcription.

### NEAT1 lncRNA sequesters SFPQ into paraspeckles away from the ADARB2 gene promoter

ADARB2 thus appears to be a paraspeckle-target gene negatively regulated by NEAT1 but positively regulated by the paraspeckle components SFPQ and hnRNPH1. We anticipated that NEAT1 up-regulation by proteasome inhibition and the ensuing sequestration of SFPQ within enlarged paraspeckles would synergize and strongly repress ADARB2 gene expression. Accordingly, qRT-PCR showed that a 17-h treatment with MG132 or bortezomib led to 10- to 20-fold-lowered ADARB2 RNA levels (Figure 7A). The down-regulation of ADARB2 gene expression likely occurs at the transcription level, since there is a comparable reduction of ADARB2 mRNA observed after 6-h MG132-treatment in both total and nascent RNA (Figure 7B). To determine whether down-regulation of ADARB2 is coupled to enlargement of paraspeckles, we measured ADARB2 mRNA levels in control (GFP) and ΔNEAT1 cells treated with MG132. The suppression of ADARB2 gene expression was significantly milder in ΔNEAT1 cells (Figure 7C), indicating that suppression of ADARB2 gene transcription by proteasome inhibition is, at least in part, NEAT1 dependent.

These data led us to propose a model to explain the negative effect of NEAT1 on ADARB2 levels: namely that NEAT1 sequesters SFPQ within paraspeckles, thereby depleting SFPQ from the nucleoplasm, limiting the availability of SFPQ to the ADARB2 gene (Figure 8A). To test this assumption, we looked at binding of SFPQ to both NEAT1 RNA and the ADARB2 gene locus. First, by RNA immunoprecipitation (RIP), we observed an increased amount of SFPQ bound to NEAT1 after MG132 treatment (Figure 8B) despite SFPQ levels remaining constant (Figure 8, B and C), although this is perhaps not surprising, given the overall increased NEAT1 levels with MG132 (e.g., Figure 3A). Of interest, the increased association of SFPQ and NEAT1 was more enhanced for a NEAT1_2-specific region (NEAT1_2#1 and NEAT1_2#2; ~3.5-fold) than in the NEAT1_1/1_2-overlapping region (NEAT1#1 and NEAT1#2; 2-fold; Figure 8A), which is relevant because NEAT1_2, and not NEAT1_1 is the critical isoform for paraspeckle formation. However, immunofluorescence and electron microscopic in situ hybridization (EM-ISH) show that both NEAT1 isoforms, even when up-regulated by MG132 treatment, were strongly enriched within the paraspeckles (Supplemental Figure S3). Next SFPQ association with the ADARB2 gene locus was investigated by ChIP. As shown in Figure 8C, SFPQ specifically associated with the ADARB2 promoter region spanning 127 nt upstream of the transcription start site (–127) in control cells; however, this association markedly dropped in MG132-treated cells (Figure 8C). These results argue that SFPQ is depleted from the ADARB2 promoter region and nucleoplasm upon MG132

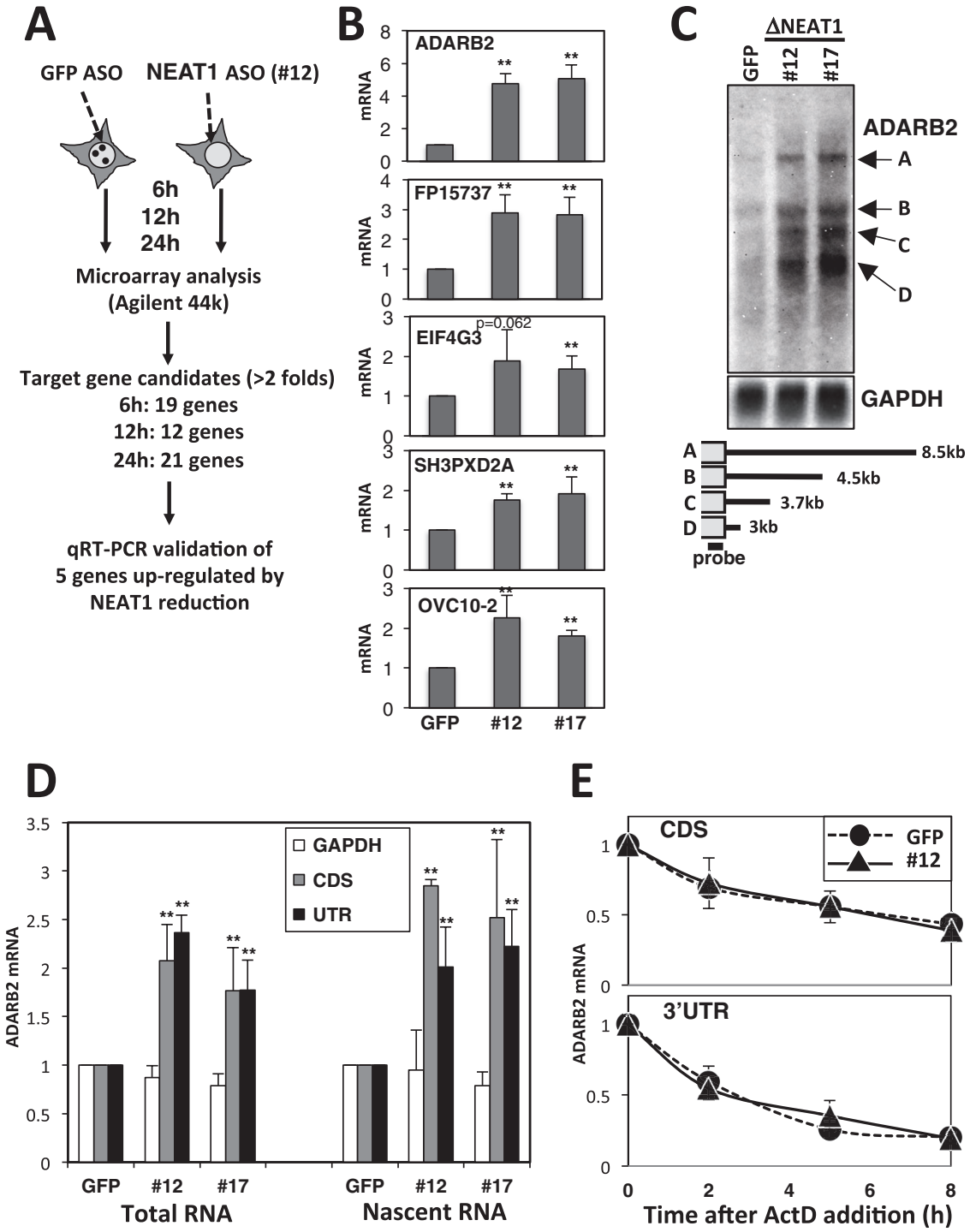


FIGURE 5: Intact paraspeckles act to suppress transcription of the ADARB2 gene. (A) Experimental strategy to identify the genes controlled by intact paraspeckles. Total RNAs were prepared from HeLa cells treated with either GFP ASO or NEAT1 ASO #12 for microarray analysis. The cells were harvested for RNA preparation 6, 12, and 24 h after ASO administration. The list of the target gene candidates is shown in Supplemental Table S1. (B) qRT-PCR validation identified five genes that were reproducibly up-regulated by two NEAT1 ASO (#12 and #17) treatments. (C) Northern blot analysis of ADARB2 mRNAs in NEAT1-eliminated cells (ΔNEAT1). PolyA+ RNAs prepared from HeLa cells treated with ASOs (green fluorescent protein [GFP] as a control, #12 and #17 for knockdown of NEAT1 lncRNA) were separated by electrophoresis on 1% agarose gels. The schematics of four putative ADARB2 mRNA isoforms (A–D) are shown. GAPDH mRNA is the loading control. (D) NEAT1 lncRNA elimination elevates the level of the nascent ADARB2 mRNA. Total RNA and pulse-labeled RNA with EU for 1 h (nascent RNA) were used as template for qRT-PCR to quantify ADARB2 mRNAs. (E) ADARB2 mRNA stability is unaltered upon NEAT1 lncRNA elimination. The mRNA decay curves (as measured by qRT-PCR) in HeLa cells treated with either GFP (solid lines) or #12 ASO (dashed lines) after actinomycin D treatment are shown. The two primer sets to detect the coding region of ADARB2 mRNA (CDS) and the 3′ UTR were used.

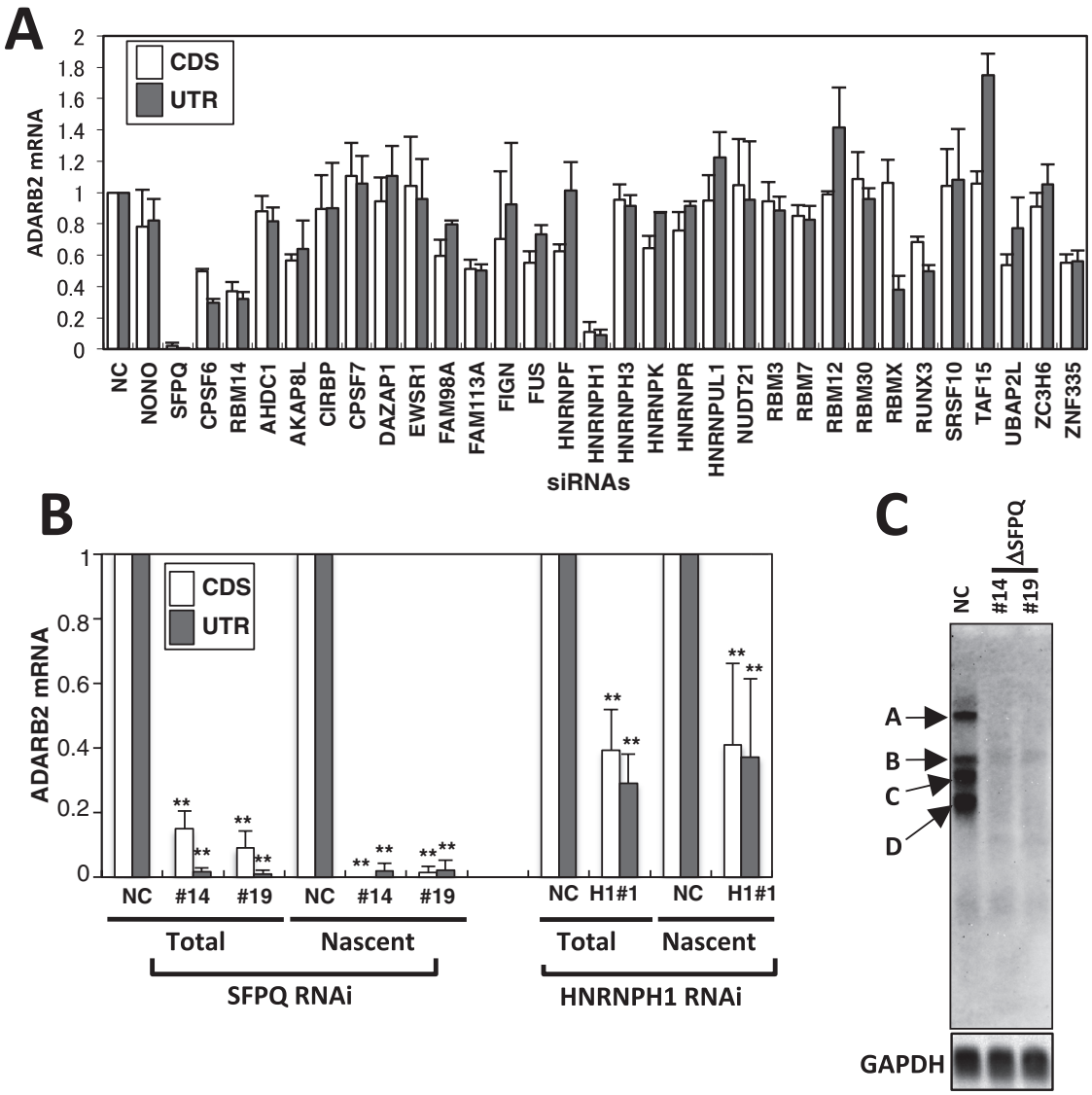


FIGURE 6: Two PSPs are required for transcription of the ADARB2 gene. (A) Identification of the PSPs required for ADARB2 gene expression. qRT-PCR to monitor ADARB2 mRNA level was carried out using RNA samples obtained from HeLa cells in which each of the PSPs was reduced by RNAi (Naganuma *et al.*, 2012). Two primer sites (CDS and UTR) were used for ADARB2 qRT-PCR. The ADARB2 mRNA level in the cells treated with control siRNA was adjusted to 1.0. The control experiment to monitor GAPDH mRNAs is shown in Supplemental Figure S6. (B) Knockdown of SFPQ and HNRNPH1 down-regulates synthesis of nascent ADARB2 mRNA. Total RNA and EU pulse-labeled RNA (nascent RNA) from control (NC) and siRNA-treated cells were used for quantification of ADARB2 mRNAs by qRT-PCR. SFPQ and HNRNPH1 were knocked down with siRNAs #14 or #19 and H1#1, respectively. (C) Northern blot analysis of ADARB2 mRNAs in control (NC) and SFPQ-knockdown (#14 and #19) cells. ADARB2 isoforms are labeled as in Figure 5C.

treatment, in parallel with elevated NEAT1 binding within elongated paraspeckles.

To determine whether this sequestration mechanism alters expression at other loci, we examined the four other selected genes (Figure 5B), which, like ADARB2, were enhanced by NEAT1 KD. Like ADARB2, these four genes were repressed to some extent by MG132, and three were dependent on SFPQ for their expression, as shown by SFPQ silencing (Figure 9). This shows that the mechanism of SFPQ sequestration by paraspeckle elongation is likely to be of general significance. The full extent of genes regulated by PSP sequestration upon proteasome inhibition is yet to be measured but is likely important, considering the diversity of transcription factors that, beyond NONO and SFPQ, are possibly trapped within enlarged paraspeckles.

### Possible role of paraspeckles in response to proteasome inhibition

In a search for cellular functions altered by enlarged paraspeckle formation in response to proteasome inhibition, we used MEFs prepared from *Neat1*$^{-/-}$ knockout mice (Neat1$^{tm1.1Shna}$; Nakagawa *et al.*, 2011). First, we confirmed that Neat1 lncRNA was also up-regulated by MG132 treatment in MEFs (Figure 10A). In particular, Neat1_2 is significantly increased after 3 and 6 h of MG132 treatment. Next we monitored the growth of Neat1$^{-/-}$ MEFs or Neat1$^{+/+}$ MEFs, treated either with DMSO (control) or MG132 over 48 h. Cell growth was measured using the xCELLigence system (Roche), which derives a "cell index" correlated with the number of cells still attached to the dish (Figure 10B). These data show that primary MEFs from both Neat1$^{-/-}$ and Neat1$^{+/+}$ mice die with MG132

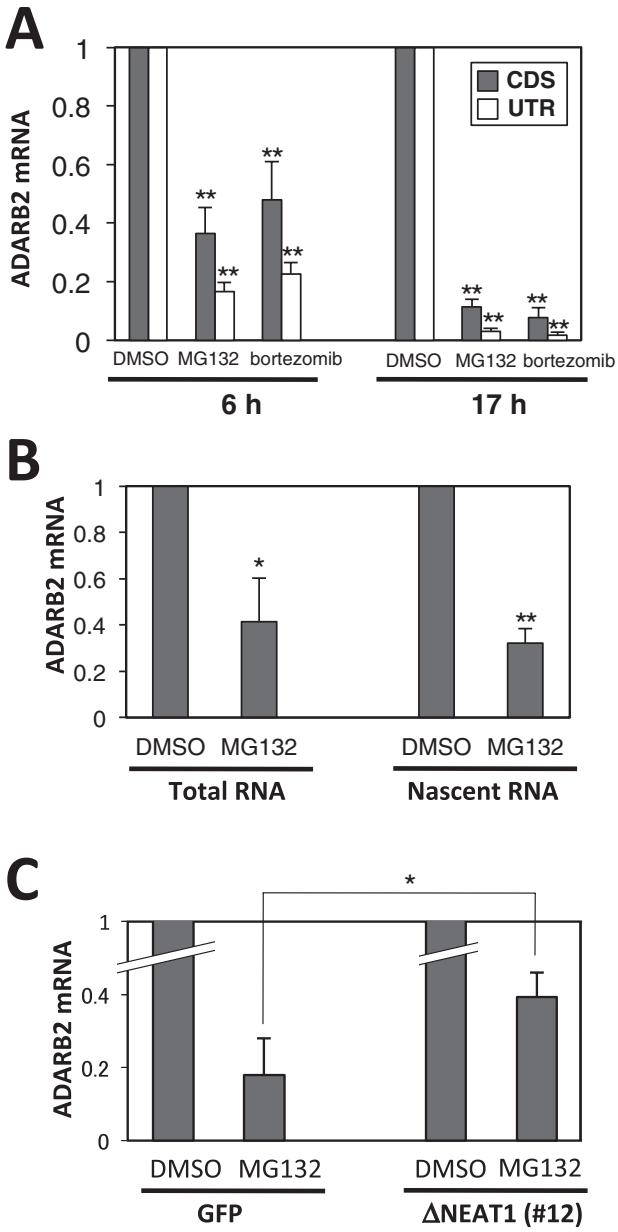


FIGURE 7: Proteasome inhibition reduces ADARB2 gene expression and requires intact paraspeckles for full suppression. (A, B) Proteasome inhibition down-regulates ADARB2 gene expression. (A) ADARB2 mRNA levels quantified by qRT-PCR from control and MG132- or bortezomib-treated HeLa cells for 6 or 17 h. (B) Proteasome inhibition (for 6 h) diminished the level of the newly synthesized nascent ADARB2 mRNA. The pulse labeling was carried out as in Figure 3C. (C) Full MG132-induced suppression of ADARB2 gene expression requires intact paraspeckles. The control (GFP) and NEAT1-eliminated (ΔNEAT1#12) cells were treated with 6 μM MG132 for 6 h. ADARB2 mRNA was monitored by qRT-PCR. $^{**}p < 0.01$, $^{*}p < 0.05$.

treatment, consistent with the induction of apoptosis under these conditions as reported previously (Jiang and Wek, 2005). Of interest, however, the MG132-treated Neat1$^{+/+}$ MEFs consistently displayed an overall less severe effect compared with the Neat1$^{-/-}$ MEFs (Figure 10B). We also noted that in the first 4 h after addition of MG132, the Neat1$^{-/-}$ MEFs started to die very quickly, with an almost immediate difference in growth for the control cells compared with the MG132-treated cells (Figure 10C; compare black and green plots). In contrast, the Neat1$^{+/+}$ MEFs had indistinguishable growth between the two treatments over the first 1–2 h of the experiment, after which they too began to die in a dose-dependent manner (Figure 10C; also Supplemental Figure S7). The effect, although transient, was consistent between experiments and different batches of MEFs (Supplemental Figure S7 shows the combined data from three biological replicates). The same pattern of more severe and quicker cell death in the NEAT1$^{-/-}$ MEFs was also obtained with different doses of bortezomib (Figure 10D) These results prompted us to determine whether the ADARB2 gene is implicated in NEAT1$^{-/-}$ cell-death sensitivity, but we could not detect ADARB2 expression in MEFs, even when NEAT1 was deleted. Thus it is likely that other genes and mechanisms are at work for a NEAT1 prosurvival role upon proteasome inhibition in MEFs. Together these cell analyses suggest an increased sensitivity of Neat1$^{-/-}$ MEFs to proteasome inhibitors, which is particularly evident in the first 2.5 h of treatment, and provide an indication that proteasome inhibitor–induced up-regulation of NEAT1 plays a role in early apoptotic defense.

## DISCUSSION

Since their discovery in 2002, the function of paraspeckles has remained largely elusive. Here we show that paraspeckles are stress-inducible structures that modulate gene expression through sequestration of transcriptional regulators (Figure 8).

### Protein sequestration within proteasome inhibition–induced elongated paraspeckles

Paraspeckles are markedly elongated as a result of NEAT1 transcriptional up-regulation upon proteasome inhibition. Our luciferase-reporter assay showed that NEAT1 promoter activity is increased in these conditions, and by I-EM we showed that elongated paraspeckles neither were enriched in ubiquitin-conjugated aggregates nor did they have an increased density of PSPs (although they do sequester a greater proportion of the total pool of PSPs due to their increased length). Thus we attribute paraspeckles enlargement to increased NEAT1 levels, consistent with reported NEAT1 up-regulation and paraspeckle enlargement taking place during in vitro myotube differentiation (Sunwoo *et al.*, 2009) and prolonged expression of a tagged NEAT1 transgene (Mao *et al.*, 2011). Our observations also provide additional evidence that NEAT1 synthesis is a rate-limiting step for paraspeckle formation. We confirm that paraspeckle width is fixed in HeLa cells, likely reflecting the molecular size of NEAT1, as we suggested previously (Souquere *et al.*, 2010), and we further show that paraspeckle length is correlated with the amount of NEAT1 transcribed within the cell. It remains to be determined how de novo paraspeckles reach their normal optimal length, presumably as part of their assembly process at the NEAT1 locus. Proteasome inhibition may lead to a delay in the timing of detachment of paraspeckles from the chromatin, thus resulting in the marked elongation of paraspeckles.

NONO and SFPQ were previously shown to be NEAT1-associated proteins (Sasaki *et al.*, 2009). Here we show by I-EM that both proteins are sequestrated within elongated paraspeckles in which the up-regulated NEAT1 transcripts accumulate upon proteasome inhibition. The intensity of this sequestration process is such that the nucleoplasmic pool of these PSPs is reduced by a factor of two. Given the variety of PSPs other than NONO and SFPQ possibly trapped within the paraspeckles in this setting, it is likely that this stress-induced sequestration mechanism has a profound influence on gene expression.

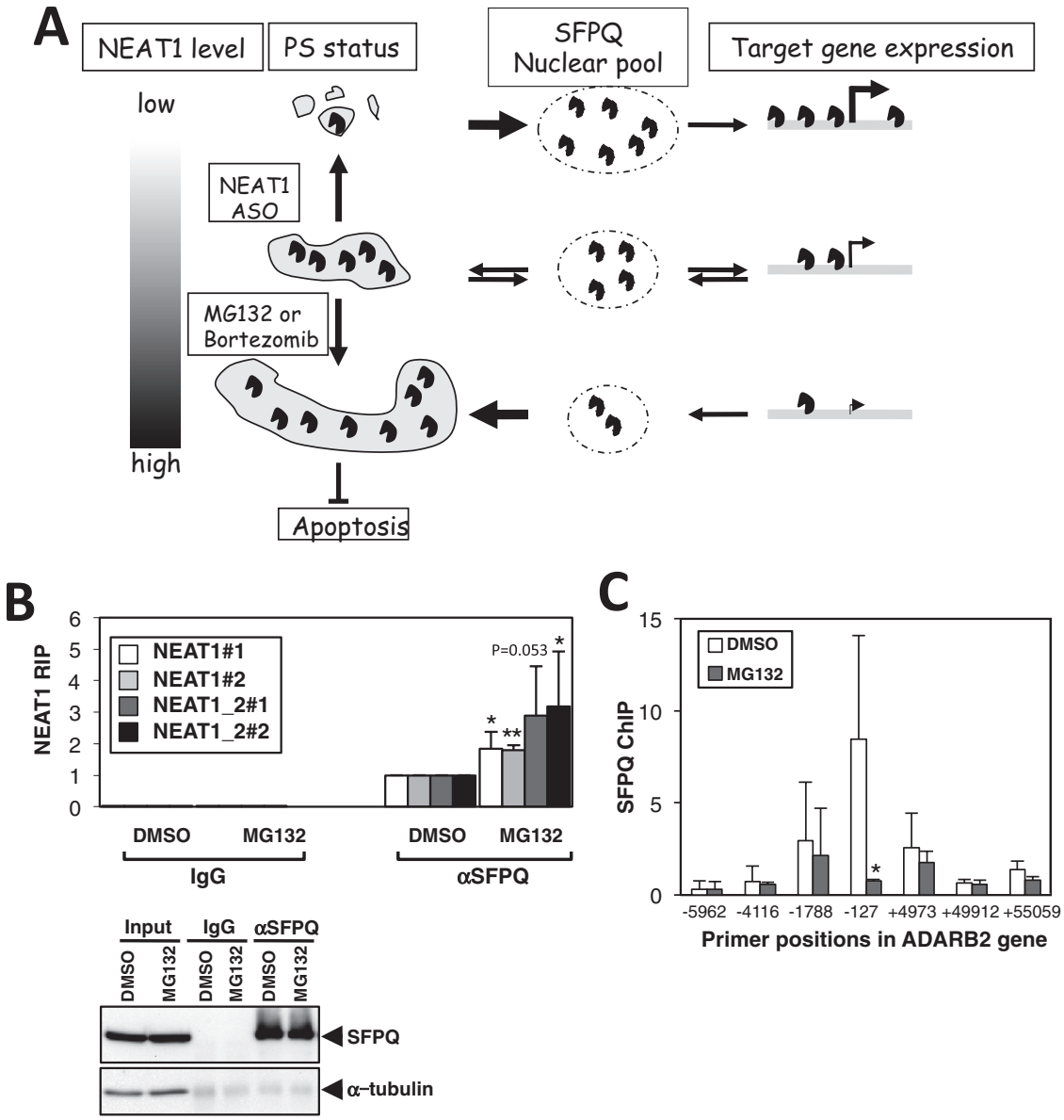


FIGURE 8: Proteasome inhibition induces SFPQ sequestration in the paraspeckles, which causes removal of SFPQ from the ADARB2 gene promoter. (A) Model of paraspeckle function. NEAT1 lncRNA expression dictates paraspeckle size and shape. NEAT1 sequesters the PSPs such as SFPQ (small black shapes) in paraspeckles. The paraspeckle unbound SFPQ is free to function as a transcriptional regulator of the several paraspeckle target genes such as ADARB2 through association with the promoters. (B) MG132 treatment results in increased association of NEAT1 RNA with SFPQ. RNA coimmunoprecipitations (RIP) with control immunoglobulin G (IgG) and anti-SFPQ (αSFPQ) were carried out from control (DMSO) and MG132-treated HeLa cells (MG132; top). The levels of coimmunoprecipitated NEAT1 lncRNAs were monitored by qRT-PCR with isoform-specific primer sets (NEAT1#1, NEAT1#2, NEAT1_2#1, and NEAT1_2#2) and normalized by immunoprecipitated SFPQ levels as shown at the bottom, in which immunoprecipitated SFPQ was quantified by Western blotting. α-Tubulin is the control. (C) Greatly reduced binding of SFPQ at the ADARB2 gene promoter in MG132-treated cells. Chromatin immunoprecipitation with αSFPQ antibody was carried out in cells treated with DMSO or MG132 for 12 h. The levels of coimmunoprecipitated DNA fragments were quantified by qPCR with the primer sets shown below, which span different segments of the ADARB2 gene locus. $^{**}p < 0.01$, $^{*}p < 0.05$.

### Identification of paraspeckle-target genes and regulation by SFPQ

Using microarrays, we show that paraspeckle disintegration by NEAT1 ASO in contrast has only minor effects on the HeLa cell transcriptome. This is surprising if one considers the many multifunctional DNA and RNA-binding proteins that are concentrated within paraspeckles as mentioned earlier. However, it is important to note that loss of "normal" (i.e., non–stress induced) paraspeckles may not have the equivalent scale of gene-regulatory effects as the gain of enlarged paraspeckles by proteasome inhibition. We can reach this conclusion because a fivefold enlargement of paraspeckles with proteasome inhibition resulted in a 50% reduction in nucleoplasmic SFPQ and NONO. Hence one could surmise that freeing SFPQ and NONO by NEAT1 ASO from "normal" paraspeckles would result in

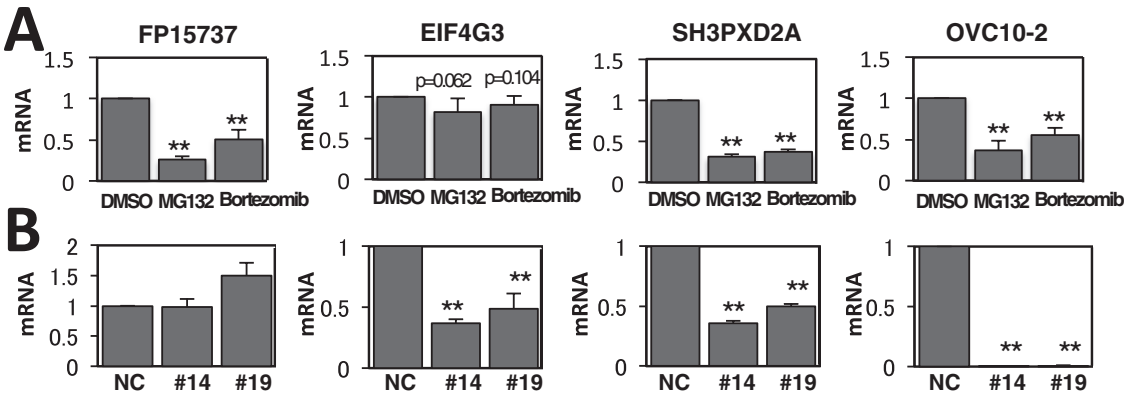


FIGURE 9: Other paraspeckle-target genes are regulated with the same molecular mechanism as for the regulation of ADARB2 gene expression. (A) Proteasome inhibition down-regulates the paraspeckle-target genes. The mRNA levels were quantified as in Figure 7A. (B) The Influence of SFPQ RNAi on mRNA accumulation of the paraspeckle-target genes was monitored by qRT-PCR. RNAi was carried out as in Figure 5B. $^{**}p < 0.01$.

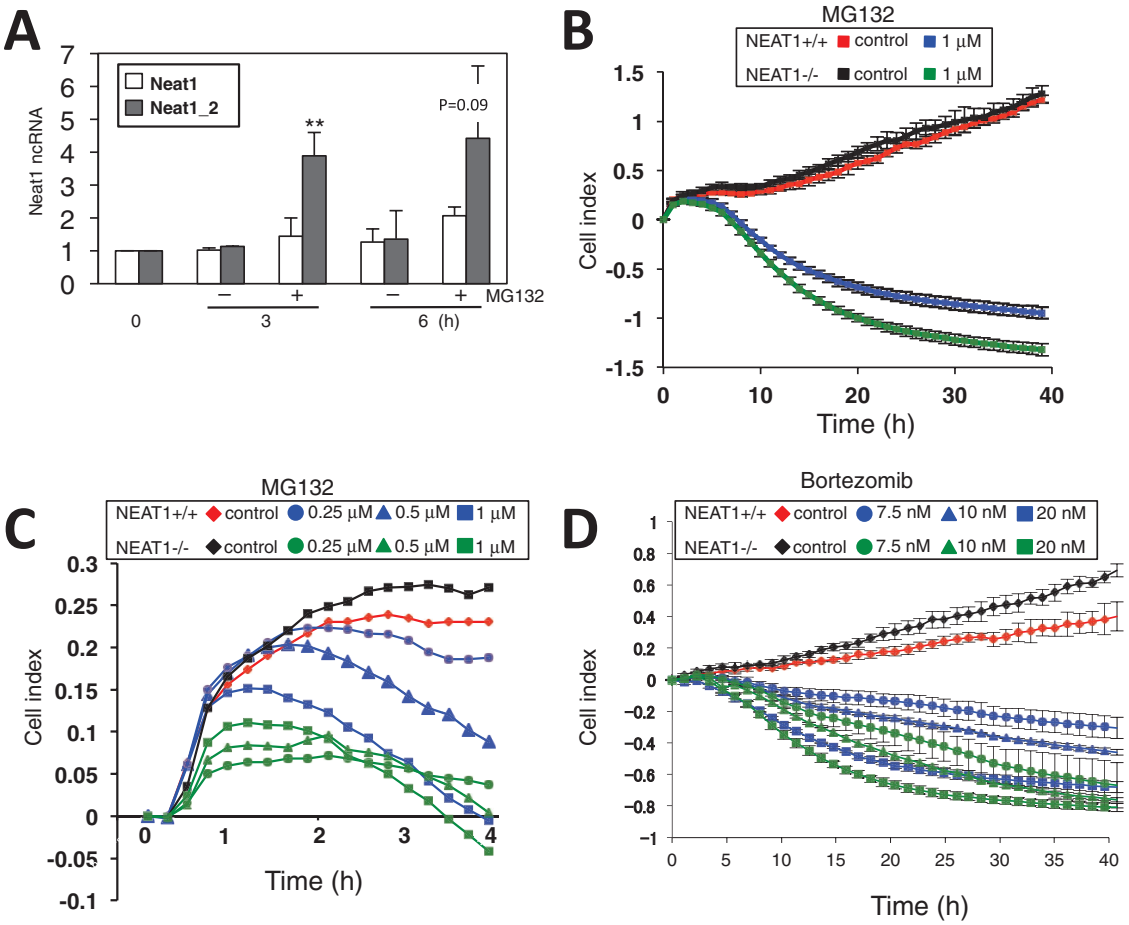


FIGURE 10: NEAT1 lncRNA acts to attenuate MG132 induced apoptosis. (A) Induction of Neat1 expression by MG132 treatment in mouse embryonic fibroblast. The Neat1 levels were quantified with two primer sets (Neat1 and Neat1_2) in MEFs treated with DMSO (–) or MG132 (+) for 0, 3, and 6 h. (B) Neat1-knockout MEFs display greater sensitivity to MG132 in real-time growth assays. Neat1$^{-/-}$ and Neat1$^{+/+}$ MEFs were analyzed in triplicate in a real-time growth assay over 40 h (Roche xCELLigence system), following the addition at time zero of 1 μM MG132 (blue for Neat1$^{+/+}$, green for Neat1$^{-/-}$) or DMSO (red for Neat1$^{+/+}$, black for Neat1$^{-/-}$) to the culture medium. Each 15-min time point is displayed; error bars are SD. (C) Neat1-knockout MEFs display a greater sensitivity to MG132 in the first 1–2 h of incubation. Experiments were performed as in B, with 0.25, 0.5, and 1 μM mG132 added to both Neat1$^{+/+}$ and Neat1$^{-/-}$ MEFs. The 15-min time points in the first 4 h are plotted. (D) Incubation of Neat1$^{+/+}$ and Neat1$^{-/-}$ MEFs with bortezomib shows a similar sensitivity of the Neat1$^{-/-}$ MEFs to proteasome inhibition relative to Neat1$^{+/+}$ MEFs. Experiment was conducted as in B, with 7.5, 10, and 20 nM bortezomib added to cells and incubated for 40 h. Error bars are SD.

a mere 10% increase in the nucleoplasmic pool of these factors, which might be insufficient to alter gene expression measurably and globally. This result, however, is consistent with the fact that the NEAT1-knockout mouse has no obvious phenotype in development and behavior (Nakagawa *et al.*, 2011). From the latter observation, it was proposed that paraspeckle function might be linked to stressful situations, including viral infections, cancer, in vitro cell differentiation, and in vitro growth of primary cells (Nakagawa and Hirose, 2012). Indeed, a recent study shows that NEAT1 is significantly up-regulated upon HIV infection and may be part of a viral defense mechanism (Zhang *et al.*, 2013). Our observations support the view that NEAT1 is induced by stress, showing that NEAT1 transcription and paraspeckle formation are enhanced by proteasome inhibition.

Despite its limitations, the NEAT1-knockdown experiment led to the identification of several paraspeckle-target genes. Among these, the ADARB2 gene was particularly intriguing as one of the three members of the adenosine deaminase family that, mostly through ADAR1 and to a lesser extent through ADARB1 activity, conducts RNA editing of various mRNAs and noncoding RNAs (ncRNAs). However, ADARB2 catalytic deaminase activity has not been detected: instead, ADARB2 is believed to function to inhibit the activity of the other ADARs in vitro (Chen *et al.*, 2000). It has been argued that paraspeckles are the retention site for ADAR RNA substrates, namely hyper–A-to-I-edited mRNAs (Prasanth *et al.*, 2005; Chen and Carmichael, 2009), raising the possibility that ADARB2 regulates nuclear ADAR activities and in turn nuclear retention of hyper-edited mRNAs in paraspeckles. However, as a word of caution, although the ADARB2 gene may play a role in HeLa cells, it is not measurably expressed in MEFs, even when NEAT1 is knocked out, indicating that its role may be restricted to human and/or transformed cells.

Because the ADARB2 gene is transcriptionally regulated by both NEAT1 and SFPQ in untreated HeLa cells, it is well suited for monitoring effects of paraspeckle elongation and loss at the level of gene transcription. In parallel to the increase of SFPQ associated with NEAT1 within the elongated paraspeckles, we measured a concomitant reduction in SFPQ bound to the ADARB2 promoter by ChIP. On the basis of that result, we propose a model of SFPQ sequestration by NEAT1 within paraspeckles that ultimately regulates ADARB2 gene expression (Figure 8A): ADARB2 is poorly expressed when more SFPQ is trapped in elongated paraspeckles (such as with MG132 treatment) and well expressed when more SFPQ is available in the nucleoplasm when paraspeckle integrity is compromised (such as after NEAT1 ASO).

There is a precedent for SFPQ behaving in a similar manner to regulate the mouse Rab23 gene, in that its binding at the promoter can be reduced by overexpression of a "competitor" retroelement lncRNA (Wang *et al.*, 2009). SFPQ possesses both RNA- and DNA-binding domains that may be responsible for binding to NEAT1 (and other) lncRNA and the promoter region of certain genes. It is interesting that of the three DBHS proteins, highly similar in sequence, SFPQ is the only one with a characterized DNA-binding domain, found within a unique N-terminus that is distinct from NONO and PSPC1. In contrast, all three DBHS proteins contain two similar RNA recognition motifs, which together fold to give a conserved dimer structure (Passon *et al.*, 2012).

The other four paraspeckle target genes described in this study include a mitochondrial iron transporter (FP15737), a translational initiation factor (eIF4G3), a Src substrate that plays a pivotal role in invadopodia formation in cancer cells (SH3PXD2A), and a zinc finger homeobox protein (OVC10-2). Under basal conditions in HeLa cells, paraspeckles likely act to subtly suppress the expression of all four genes, and this is reinforced by even further suppression with paraspeckle enlargement upon proteasome inhibition. Furthermore, three of these four genes (SH3PXD2A, OVC10-2, and EIF4G3) depend on SFPQ for their expression, whereas FP15737 is independent but could be controlled by sequestration of another PSP. It would be intriguing to investigate whether paraspeckle disintegration and/or enlargement influence the regulatory pathways in which these target genes are involved.

### Proteasome inhibition and apoptosis

We show that NEAT1 transcription and paraspeckle assembly are responsive elements when protein degradation is impeded. Moreover, when these two closely linked processes were prevented as in the NEAT1$^{-/-}$ MEFs, the resistance of the cells to proteasome inhibitor–induced cell death was clearly transiently reduced. Thus NEAT1 and paraspeckles are needed for the cells to survive when facing accumulation of undegraded proteins, at least in an initial phase of accumulation compatible with cell survival.

Our demonstration that NEAT1 is transcriptionally up-regulated by MG132 adds to the list of genes that have been shown to be induced by proteasome inhibition, including the proteasome subunit genes, which is known as the proteasome recovery pathway. This pathway is spearheaded by transcriptional activation by a variety of factors. In mammalian cells, the specific transcription factor Nrf1 was identified to mediate this response (Radhakrishnan *et al.*, 2010). In contrast, transcriptional induction of the cyclooxygenase-2 gene induced by proteasome inhibition requires reactive oxygen species–dependent protein kinases and transcription factors CCAAT/enhancer-binding protein δ and its coactivator cAMP-response element-binding protein (CREB)–binding protein (Chen *et al.*, 2005). In the case of the NEAT1 gene, future identification of the signaling pathway responsible for transcriptional activation in response to proteasome inhibition will be guided by analyses of the promoter that contains potential binding sites of numerous transcription factors, including CREB and nuclear factor κB (NFκB).

Prolonged proteasome inhibition triggers apoptosis, believed to be induced by several events, including inhibition of the phosphoinositide 3-kinase/Akt and NFκB pathways and activation of the p38-JNK1/2 pathway (Zanotto-Filho *et al.*, 2012). It was also reported that failure of amino acid homeostasis caused cell death after proteasome inhibition (Suraweera *et al.*, 2012). We showed here that NEAT1 induction and the subsequent enlargement of paraspeckles is not a futile side effect induced by proteasome inhibition, but instead is an element in the cellular response to stress. The higher sensitivity toward proteasome inhibition of NEAT1-deficient cells suggests an antiapoptotic function mediated by paraspeckle formation. Of interest, in adult mouse tissues, paraspeckle formation occurs in restricted cell types, in particular within the epithelia of the gastrointestinal tract, where paraspeckles are observed in differentiated cells at the tips of crypts where apoptosis is occurring (Nakagawa *et al.*, 2011). Further studies are needed to expand our understanding of the roles that NEAT1 and the paraspeckles play in modulating entry to apoptosis in response to stress and how this is related to changes in gene expression profiles mediated by PSP sequestration.

## MATERIALS AND METHODS

### Cell culture

HeLa cells were cultured in DMEM/10% fetal calf serum (FCS) at 37°C with 5% $CO_2$. MEFs from NEAT1$^{+/+}$ and NEAT1$^{-/-}$ mouse embryos (Nakagawa *et al.*, 2011) were cultured in DMEM/F-12/10% FCS (Life Technologies, Carlsbad, CA) at 37°C with 5% $CO_2$. The

cells were treated with proteasome inhibitors in culture medium at concentrations of 5 mM and 0.25, 0.5, and 1 μM for MG132 in HeLa and MEF, respectively, and concentrations of 100 nM and 7.5, 10, and 20 nM for bortezomib in HeLa and MEF, respectively. DMSO equivalent to the highest drug concentration was added as negative control treatment.

### Cell fractionation

We followed the nucleolar isolation protocol developed by the Lamond lab (www.lamondlab.com/f7nucleolarprotocol.htm). HeLa nuclei were prepared from $1 \times 10^8$ cells, then washed three times with phosphate-buffered saline (PBS), resuspended in 5 ml of buffer A (10 mM 4-(2-hydroxyethyl)-1-piperazineethanesulfonic acid, pH 7.9, 10 mM KCl, 1.5 mM $MgCl_2$, 0.5 mM dithiothreitol), and homogenized for 10 strokes using a Dounce homogenizer with a tight pestle. An aliquot of the homogenate was removed as a source for the total RNA. The rest of the homogenate was centrifuged at $218 \times g$ for 5 min at 4°C, yielding cytosolic (supernatant) fractions. The pellet was resuspended in 3 ml of S1 solution (0.25 M sucrose, 10 mM $MgCl_2$), overlaid onto 3 ml of S2 solution (0.35 M sucrose, 0.5 mM $MgCl_2$), and centrifuged at $1430 \times g$ for 5 min at 4°C. The pellet was resuspended in 3 ml of S2 solution, and an aliquot was removed as the nuclear fraction. The rest of the suspension was sonicated by repeating 5-s pulses 20 times, using a hand sonicator equipped with a microprobe (UR-20P; TOMY Seiko, Tokyo, Japan) at 80% of the maximum output. Sonicate was overlaid onto equal volumes of S3 solution (0.88 M sucrose, 0.5 mM $MgCl_2$). Before centrifugation, the border of the two layers was marked. The solution was then centrifuged at $5000 \times g$ for 10 min at 4°C, resulting in two layers of supernatant (Np1 and Np2) and one pellet layer (No). The pellet was rinsed with S2 solution and recovered by centrifugation. The resulting pellet, together with previously obtained fractions, was subjected to RNA extraction.

### RNA interference

HeLa cells were transfected with siRNAs at 33 nM (final concentration) by using Lipofectamine RNAiMAX according to the manufacturer's instructions (Invitrogen). After 48 h, the cells were again transfected and incubated for 48 h. Knockdown efficiencies were verified by qRT-PCR or Western blotting. Stealth siRNAs for PSPs and the negative control were purchased from Invitrogen. The siRNA sequences used in this study are shown in Supplemental Table S3.

### Capture of nascent RNAs

To capture nascent RNAs, 0.5 mM EU was added into the culture medium and was incorporated into the cells for 30 min. Total RNA was prepared with TRIzol reagent (Invitrogen). The EU-labeled RNAs were biotinylated and captured by using the Click-it Nascent RNA Capture Kit (Life Technologies), in accordance with the manufacturer's instructions. A 1-μg amount of EU-labeled RNA was biotinylated with 0.5 mM biotin azide in Click-iT reaction buffer. The biotinylated RNAs were precipitated with ethanol and resuspended in distilled water. The biotinylated RNAs mixed with Dynabeads MyOne Streptavidin T1 magnetic beads in Click-iT RNA binding buffer and heated at 68°C for 5 min, followed by incubation at room temperature for 30 min while gently vortexing. The beads were immobilized using the DynaMag-2 magnet and were washed with Click-iT wash buffer1 and 2. The washed beads were resuspended in Click-iT wash buffer2 and used for cDNA synthesis.

### qRT-PCR and reporter gene assays

qRT-PCR was performed as described previously (Sasaki *et al.*, 2009). Total RNA was prepared from cell culture using TRIzol reagent (Life Technologies). The total RNA (500 ng) or the nascent RNA was reverse transcribed using QuantiTect reverse transcription kit (Qiagen, Venlo, Netherlands). The primers were designed by Primer3 software (www-genome.wi.mit.edu/ftp/distribution/software/) and purchased from Invitrogen. Aliquots of cDNA were subjected to real-time PCR, performed using a Lightcycler 480 SYBR Green I Master (Roche, Basel, Switzerland) according to the manufacturer's protocol. Primers used are shown in Supplemental Table S5.

For luciferase reporter assays, the human NEAT1 promoter (hg18 coordinates 64940168-64946905) was amplified from human genomic DNA and inserted into the pGL3 plasmid (Promega, Fitchburg, WI) with *Kpn*I and *Nhe*I. pGL3-NEAT1promoter and pGL3-SV40 promoter (Promega) were transfected into HeLa cells with Lipofectamine 2000 (Life Technologies) and 5 μM MG132 or equivalent DMSO added 24 h later. After a 17-h incubation, RNA was harvested and reverse transcribed, and levels of luciferase RNA and GAPDH were measured using qPCR.

### Northern and Western blotting

For Northern blot hybridization, total RNA was separated by electrophoresis in 1% agarose gel containing 2% formaldehyde, followed by blotting to a positively charged nylon membrane (Roche). The blotted RNAs were fixed to the membrane by ultraviolet irradiation. Antisense RNA probes were synthesized with the DIG Easy Hyb RNA labeling kit (Roche) and hybridized with the DIG Easy Hyb reagent overnight at 68°C. The membrane was washed, and the hybridized bands were detected with the DIG Wash and Block buffer set (Roche). For Western blotting, the total cell lysate was run on an 8% SDS–PAGE gel and then blotted on a polyvinylidene fluoride membrane. The antibodies used are shown in Supplemental Table S2.

### RNase protection assay

Total RNA was prepared with TRIzol reagent (Life Technologies). The RNase protection assay was performed with the RPAIII kit (Ambion, Austin, TX), according to the manufacturer's protocol. A 3-μg amount of total RNA was hybridized with a $^{32}P$-labeled antisense RNA probe that was synthesized with T7 RNA polymerase (TaKaRa, Kyoto, Japan) at 42°C for ~18 h. RNase A/T1 digestion (×100 dilution of the master mix solution) excluded unhybridized single-stranded RNA probes. The protected RNA fragments were separated by 6% PAGE containing 7 M urea. Radioactive RNA bands were visualized and quantified with the Bioimaging analyzer BAS3000.

### ASO administration into cells

The antisense chimeric oligonucleotides used for knockdown experiments were phosphothioate modified at their backbone to increase their stability. Five terminal nucleotides from the 5′ and 3′ ends were substituted by 2′-*O*-methylribonucleotides. NEAT1 ASO #12 and #17 are targeted to +1422 and +410 in the region common to NEAT1_1 and NEAT1_2 isoforms. The sequences of the ASOs used in this study are shown in Supplemental Table S4. The trypsinized HeLa cells ($1 \times 10^6$ cells) were suspended in 100 μl of Solution R of the Cell Line Nucleofector Kit R (Lonza, Basel, Switzerland) and then mixed with oligonucleotides (4 μM final concentration). Transfection was carried out in an electroporation cuvette using the Nucleofector instrument (Lonza). The transfected cells were transferred to fresh DMEM plus 10% fetal bovine serum and incubated at 37°C and 5% $CO_2$ for 24 h, followed by harvesting cells for RNA preparation.

### DNA microarray

HeLa cells were nucleofected with GFP ASO or NEAT1 ASO (#12) and incubated for 6, 12, and 24 h. Total RNA was then prepared and

labeled with Cy3. Samples were hybridized to a Human Oligo Microarray (G4112F; Agilent, Santa Clara, CA) according to the manufacturer's protocol. Arrays were scanned with a G2565BA Microarray Scanner System (Agilent), and the resulting data were analyzed using the GeneSpring GX software (Agilent). The raw data are available in Gene Expression Omnibus (www.ncbi.nlm.nih.gov/geo/info/linking.html, accession number GSE45158).

### Chromatin immunoprecipitation assay

HeLa cells were fixed with 1% formaldehyde for 10 min, after which the cross-linking was stopped by treatment with 125 mM glycine for 5 min. The fixed cells were lysed in cell lysis buffer (10 mM Tris-HCl, pH 8.0, 10 mM NaCl, 0.5% NP40) for 10 min on ice. The lysed cells were centrifuged to recover the nuclear pellet, which was suspended in nuclear lysis buffer (50 mM Tris-HCl, pH 8.0, 10 mM EDTA, 1% SDS). The nuclear lysate was sonicated with Bioruptor UCW-310 (Diagnode, Liège, Belgium) to make average DNA fragment sizes of 500 base pairs. After the cell debris was removed by centrifugation at 20,000 *g* for 10 min at 8°C, the supernatants were diluted with a 10-fold volume of dilution buffer (16.7 mM Tris-HCl, pH 8.0, 167 mM NaCl, 1.2 mM EDTA, pH 8.0, 1.1% Triton X-100). Chromatin was immunoprecipitated overnight with anti-RNAPII or anti-SFPQ antibodies conjugated with Dynabeads–mouse immunoglobulin G or Dynabeads–protein G (Life Technologies), respectively. The recovered beads were washed once with wash buffer 1 (20 mM Tris-HCl, pH 8.0, 150 mM NaCl, 2 mM EDTA pH 8.0, 1% Triton X-100, and 0.1% SDS), once with wash buffer 2 (20 mM Tris-HCl, pH 8.0, 500 mM NaCl, 2 mM EDTA, pH 8.0, 1% Triton X-100, and 0.1% SDS), and once with wash buffer 3 (20 mM Tris-HCl, pH 8.0, 500 mM LiCl, 2 mM EDTA, pH 8.0, 1% Triton X-100, and 0.1% SDS). The captured chromatin was eluted and reverse cross-linked in elution buffer (25 mM Tris-HCl, pH 8.0, 5 mM EDTA, 0.5% SDS, and 0.1 mg/ml protease K) at 65°C for 6 h and then treated with 50 μg/ml RNase A at 37°C for 30 min. The precipitated DNAs were used for qPCR. The primers used are shown in Supplemental Table S5.

### Immunoprecipitation

HeLa cells ($2 \times 10^6$ cells) were lysed with lysis buffer (50 mM Tris-HCl, pH 7.5, 150 mM NaCl, 1 mM EDTA, and 1% Triton X-100) for 30 min on ice, and the cell extract (1 mg of protein) was used for immunoprecipitation (IP) experiments. Protein complexes were precipitated with an antibody against SFPQ conjugated to Dynabeads–protein G beads (Life Technologies) for 1 h at room temperature. The IP products were washed four times with lysis buffer. Detailed information about the antibodies used is shown in Supplemental Table S2.

### Immunofluorescence

HeLa cells were fixed with 4% paraformaldehyde/PBS. Fixed cells were permeabilized with 0.2% Triton X-100/PBS for 5 min, rinsed, and blocked with 10% normal horse serum (Vector Laboratories, Burlingame, CA) in PBS for 1 h. Primary antibodies were applied for 1 h at room temperature or overnight at 4°C. The samples were washed three times with PBST (PBS, 0.1% Tween-20) for 5 min each. Secondary antibodies were applied for 1 h at room temperature. After washing, the slides were cover slipped with Vectashield (Vector Laboratories) containing 4′,6-diamidino-2-phenylindole (DAPI). Fluorescence images were visualized by microscopy at room temperature on a microscope (FluoView FV1000D IX81; Olympus, Tokyo, Japan) equipped with U-Plan Apochromat 40×/0.95 objective lenses (Olympus). FluoView FV10-ASW1.7 software (Olympus) was used for image acquisition and processing. All overlaid images were transferred as high-resolution JPEG files. Figures were compiled using Photoshop (Adobe Systems, San José, CA). The antibodies used are shown in Supplemental Table S2.

### RNA fluorescence in situ hybridization

Cells were seeded onto a multichamber culture slide (Corning, Corning, NY) and fixed with 4% paraformaldehyde/PBS. The fixed cells were permeabilized with 0.5% Triton X-100/PBS for 5 min. RNA probes were prepared using a DIG/FITC RNA Labeling Kit (Roche Diagnostic) according to the manufacturer's protocols. Dehydrated slides were incubated for 16 h at 55°C with a hybridization solution (2× saline–sodium citrate [SSC], 50% formamide, 1× Denhardt's salt [Sigma-Aldrich, St. Louis, MO], 10 mM EDTA, 100 μg/ml yeast tRNA, 0.01% Tween-20, and 5% dextran sulfate) containing digoxigenin- or fluorescein isothiocyanate–labeled RNA probe. The slides were washed twice with prewarmed wash buffer (2× SSC, 50% formamide, and 0.01% Tween-20) at 55°C for 30 min. Excess RNA probes were digested with 10 μg/ml RNase A in NTET (10 mM Tris-HCl, pH 8.0, 1 mM EDTA, 500 mM NaCl, and 0.1% Tween-20) at 37°C for 1 h. The slides were washed with buffer (2× SSC, 0.01% Tween-20) at 55°C for 30 min and twice with a second buffer (0.1× SSC, 0.01% Tween-20) at 55°C for 30 min. After washing, the slides were cover slipped with Vectashield (Vector Laboratories) containing DAPI.

### Electron microscopic studies

Conventional ultrastructural microscopy after Epon embedding was as in Souquere *et al*. (2009). Thin sections were analyzed with a FEI Tecnai Spirit, and digital images were taken with a SIS MegaviewIII charge-coupled device camera. Paraspeckle frequency was established by counting paraspeckle sections within 10 squares of 200-mesh EM grids for samples of control ($5.6 \pm 2.8$ paraspeckles/square) and MG132-treated HeLa cells ($19 \pm 6.1$ paraspeckles/square) with similar cell densities (cell pellets). When coupled to the 50% increase of the mean length of the paraspeckles (as in Figure 1C), this indicates a 5.1-fold increase of paraspeckle surface after 17-h, 5 μM MG132 treatment. Immuno–electron microscopic studies were as in Souquere *et al*. (2010). Data were obtained on paraformaldehyde-fixed HeLa cells except for anti-PML immunodetection, which was carried out on glutaraldehyde-fixed HeLa cells. The primary antibodies used for immunodetection are listed in Supplemental Table S1. Anti-mouse or anti-rabbit secondary antibodies coupled to 10-nm gold particles were from BBInternational (Cardiff, UK). For quantification of labeling densities, control and MG132-treated cells were processed in parallel from chemical fixation to Lowicryl embedding and to final incubation with antibodies. Gold particles were counted by eye. Surface areas were determined with analySIS. Calculations and standard deviations were obtained with Excel (Microsoft, Redmond, WA). Electron microscopic in situ hybridizations were as in Souquere *et al*. (2010), except that duration of dUTP biotinylation of DNA probes by nick translation was reduced to 30 min.

### Monitoring cell death

Roche's xCELLigence System for real-time cell analysis (which measures impedance-based signals) was used to quantify cell proliferation. Several different preparations of Neat1$^{-/-}$ and Neat1$^{+/+}$ MEFs, each from different individual knockout mice and wild-type littermates (Nakagawa *et al*., 2011), were cultured in DMEM/F-12 (Life Technologies), supplemented with 10% FCS (Life Technologies). On the day before the experiment, cells were detached with triple Xpress (Life Technologies), and $2.5 \times 10^3$ viable cells were plated in individual wells of an E-16 xCELLigence plate (xCELLigence, Roche, Germany) in a 100-μl volume of culture medium. Cells were left to settle for 24 h in the incubator, followed by the addition of 100 μl of

prewarmed MG132, bortezomib, or DMSO (diluted in culture medium) to each well as appropriate, with each drug treatment on each cell type being carried out in triplicate. The plate was immediately inserted into the xCELLigence apparatus inside an incubator, and electrical impedance was measured across the bottom of each well in real time every 15 min for 40 h according to the manufacturer's recommendations.

## ACKNOWLEDGMENTS

We thank the members of the Hirose, Fox, and Pierron laboratories. G.V. was supported by an Erasmus exchange program with the University of Naples (Naples, Italy). This research was supported by the Funding Program for Next Generation World-Leading Researchers of the Japan Society for the Promotion of Science (to T.H.) and by grants from the New Energy and Industrial Technology Development Organization (to T.H.), the Takeda Science Foundation (to T.H.), the National Health and Medical Research Council of Australia (to A.H.F.), the Medical Research Foundation of Royal Perth Hospital (to A.H.F), and the Centre National de la Recherche Scientifique and the Association pour la Recherche sur le Cancer (to G.P.).

## REFERENCES

Bond CS, Fox AH (2009). Paraspeckles: nuclear bodies built on long noncoding RNA. J Cell Biol 186, 637–644.

Chen CX, Cho DS, Wang Q, Lai F, Carter KC, Nishikura K (2000). A third member of the RNA-specific adenosine deaminase gene family, ADAR3, contains both single- and double-stranded RNA binding domains. RNA 6, 755–767.

Chen JJ, Huang WC, Chen CC (2005). Transcriptional regulation of cyclooxygenase-2 in response to proteasome inhibitors involves reactive oxygen species-mediated signaling pathway and recruitment of CCAAT/enhancer-binding protein delta and CREB-binding protein. Mol Biol Cell 16, 5579–5591.

Chen LL, Carmichael GG (2009). Altered nuclear retention of mRNAs containing inverted repeats in human embryonic stem cells: functional role of a nuclear noncoding RNA. Mol Cell 35, 467–478.

Clemson CM, Hutchinson JN, Sara SA, Ensminger AW, Fox AH, Chess A, Lawrence JB (2009). An architectural role for a nuclear noncoding RNA: NEAT1 RNA is essential for the structure of paraspeckles. Mol Cell 33, 717–726.

Clemson CM, McNeil JA, Willard HF, Lawrence JB (1996). XIST RNA paints the inactive X chromosome at interphase: evidence for a novel RNA involved in nuclear/chromosome structure. J Cell Biol 132, 259–275.

Dong X, Sweet J, Challis JR, Brown T, Lye SJ (2007). Transcriptional activity of androgen receptor is modulated by two RNA splicing factors, PSF and p54nrb. Mol Cell Biol 27, 4863–4875.

Fox AH, Bond CS, Lamond AI (2005). P54nrb forms a heterodimer with PSP1 that localizes to paraspeckles in an RNA-dependent manner. Mol Biol Cell 16, 5304–5315.

Fox AH, Lam YW, Leung AK, Lyon CE, Andersen J, Mann M, Lamond AI (2002). Paraspeckles: a novel nuclear domain. Curr Biol 12, 13–25.

Heyd F, Lynch KW (2010). Phosphorylation-dependent regulation of PSF by GSK3 controls CD45 alternative splicing. Mol Cell 40, 126–137.

Hutchinson JN, Ensminger AW, Clemson CM, Lynch CR, Lawrence JB, Chess A (2007). A screen for nuclear transcripts identifies two linked noncoding RNAs associated with SC35 splicing domains. BMC Genomics 8, 39.

Jiang HY, Wek RC (2005). Phosphorylation of the α-subunit of the eukaryotic initiation factor-2 (eIF2α) reduces protein synthesis and enhances apoptosis in response to proteasome inhibition. J Biol Chem 280, 14189–14202.

Kaneko S, Rozenblatt-Rosen O, Meyerson M, Manley JL (2007). The multifunctional protein p54nrb/PSF recruits the exonuclease XRN2 to facilitate pre-mRNA 3′ processing and transcription termination. Genes Dev 21, 1779–1789.

Li S, Kuhne WW, Kulharya A, Hudson FZ, Ha K, Cao Z, Dynan WS (2009). Involvement of p54(nrb), a PSF partner protein, in DNA double-strand break repair and radioresistance. Nucleic Acids Res 37, 6746–6753.

Mao YS, Sunwoo H, Zhang B, Spector DL (2011). Direct visualization of the co-transcriptional assembly of a nuclear body by noncoding RNAs. Nat Cell Biol 13, 95–101.

Naganuma T, Nakagawa S, Tanigawa A, Sasaki Y, Goshima N, Hirose T (2012). Alternative 3′-end processing of long noncoding RNAs initiates construction of nuclear paraspeckles. EMBO J 31, 4020–4034.

Nakagawa S, Hirose T (2012). Paraspeckle nuclear bodies–useful uselessness. Cell Mol Life Sci 69, 3027–3036.

Nakagawa S, Naganuma T, Shioi G, Hirose T (2011). Paraspeckles are subpopulation-specific nuclear bodies that are not essential in mice. J Cell Biol 193, 31–39.

Passon DM, Lee M, Rackham O, Stanley WA, Sadowska A, Filipovska A, Fox AH, Bond CS (2012). Structure of the heterodimer of human NONO and paraspeckle protein component 1 and analysis of its role in subnuclear body formation. Proc Natl Acad Sci USA 109, 4846–4850.

Prasanth KV, Prasanth SG, Xuan Z, Hearn S, Freier SM, Bennett CF, Zhang MQ, Spector DL (2005). Regulating gene expression through RNA nuclear retention. Cell 123, 249–263.

Radhakrishnan SK, Lee CS, Young P, Beskow A, Chan JY, Deshaies RJ (2010). Transcription factor Nrf1 mediates the proteasome recovery pathway after proteasome inhibition in mammalian cells. Mol Cell 38, 17–28.

Saha S, Murthy S, Rangarajan PN (2006). Identification and characterization of a virus-inducible non-coding RNA in mouse brain. J Gen Virol 87, 1991–1995.

Sasaki YT, Ideue T, Sano M, Mituyama T, Hirose T (2009). MENepsilon/beta noncoding RNAs are essential for structural integrity of nuclear paraspeckles. Proc Natl Acad Sci USA 106, 2525–2530.

Shav-Tal Y, Zipori D (2002). PSF and p54(nrb)/NonO–multi-functional nuclear proteins. FEBS Lett 531, 109–114.

Sone M, Hayashi T, Tarui H, Agata K, Takeichi M, Nakagawa S (2007). The mRNA-like noncoding RNA Gomafu constitutes a novel nuclear domain in a subset of neurons. J Cell Sci 120, 2498–2506.

Souquere S, Beauclair G, Harper F, Fox A, Pierron G (2010). Highly ordered spatial organization of the structural long noncoding NEAT1 RNAs within paraspeckle nuclear bodies. Mol Biol Cell 21, 4020–4027.

Souquere S, Mollet S, Kress M, Dautry F, Pierron G, Weil D (2009). Unravelling the ultrastructure of stress granules and associated P-bodies in human cells. J Cell Sci 22, 3619–3626.

Spector DL (2006). SnapShot: cellular bodies. Cell 127, 1071.

Sunwoo H, Dinger ME, Wilusz JE, Amaral PP, Mattick JS, Spector DL (2009). MEN epsilon/beta nuclear-retained non-coding RNAs are up-regulated upon muscle differentiation and are essential components of paraspeckles. Genome Res 19, 347–359.

Suraweera A, Münch C, Hanssum A, Bertolotti A (2012). Failure of amino acid homeostasis causes cell death following proteasome inhibition. Mol Cell 48, 242–253.

Tripathi V *et al*. (2010). The nuclear-retained noncoding RNA MALAT1 regulates alternative splicing by modulating SR splicing factor phosphorylation. Mol Cell 39, 925–938.

Visa N, Puvion-Dutilleul F, Bachellerie JP, Puvion E (1993). Intranuclear distribution of U1 and U2 snRNAs visualized by high resolution in situ hybridization: revelation of a novel compartment containing U1 but not U2 snRNA in HeLa cells. Eur J Cell Biol 60, 308–321.

Wang G, Cui Y, Zhang G, Garen A, Song X (2009). Regulation of proto-oncogene transcription, cell proliferation, and tumorigenesis in mice by PSF protein and a VL30 noncoding RNA. Proc Natl Acad Sci USA 106, 16794–16798.

Yang L, Lin C, Liu W, Zhang J, Ohgi KA, Grinstein JD, Dorrestein PC, Rosenfeld MG (2011). ncRNA- and Pc2 methylation-dependent gene relocation between nuclear structures mediates gene activation programs. Cell 147, 773–788.

Zanotto-Filho A, Braganhol E, Battastini AM, Moreira JC (2012). Proteasome inhibitor MG132 induces selective apoptosis in glioblastoma cells through inhibition of PI3K/Akt and NFkappaB pathways, mitochondrial dysfunction, and activation of p38-JNK1/2 signaling. Invest New Drugs 10, 1007.

Zhang O, Chen CY, Yedevalli VS, Jeang KT (2013). NEAT1 long noncoding RNA and paraspeckle bodies modulate HIV-1 posttranscriptional expression. MBio 4, e00596–12.

Zheng R, Shen Z, Tripathi V, Xuan Z, Freier SM, Bennett CF, Prasanth SG, Prasanth KV (2010). Polypurine-repeat-containing RNAs: a novel class of long non-coding RNA in mammalian cells. J Cell Sci 123, 3734–3744.